

Activated Boron Nitride Derived from Activated Carbon

Wei-Qiang Han,^{†,‡} R. Brutchey,[§] T. D. Tilley,[§] and A. Zettl^{*,†,‡}

Department of Physics, University of California, Berkeley, California 94720, and Molecular Foundry, Materials Sciences Division, Lawrence Berkeley National Laboratory, Berkeley, California 94720, and Department of Chemistry, University of California, Berkeley, California 94720

Received September 30, 2003; Revised Manuscript Received October 31, 2003

ABSTRACT

An activated carbon template substitution reaction has been used to synthesize activated boron nitride (BN). The resulting material is characterized by scanning electron microscopy, high-resolution transmission electron microscopy, electron energy loss spectroscopy, and surface area analysis. The activated BN microstructure is similar to that of the starting activated carbon template. The specific surface area, total pore volume, and average pore radius of template-derived activated BN are 168 m²/g, 0.27 cm³/g, and 32.2 Å, respectively.

Porous solids have applications ranging from adsorbents to purification chromatographic packing to support structures for catalytic processes. A wide variety of porous solids exist, including zeolites, pillared clays, porous polymeric solids, and porous carbon.¹ Among these, porous carbon, often called activated carbon, displays exceptional porosity, extended surface area, universal adsorption capability, high adsorption capacity, and a high degree of surface reactivity. In the broadest sense, activated carbon can be defined as an amorphous carbon-based material with a high degree of porosity and an extended interparticulate surface area; often the microscopic structure can be visualized as stacks of flat aromatic sheets cross-linked in a random manner.² Activated carbon is currently the most economic and popularly used porous solid.²

Hexagonal boron nitride (BN), a material structurally closely related to graphite, has an attractive combination of chemical, thermal, and electrical properties. The utility of activated carbon suggests that an analogous “activated” BN exhibiting a high degree of porosity and an extended interparticulate surface area might be of scientific and economic importance. Although conventionally produced film and particle forms of BN are nonporous,³ some progress^{4–6} has been made in synthesizing enhanced porosity. Unfortunately, the associated synthesis routes for enhanced-porosity BN typically employ borane-based molecular precursors, which are both expensive and highly toxic, making these routes unattractive for high volume production.

We here explore an alternate method for activated BN synthesis. It has been previously shown that BN⁷ and B_xC_yN_z^{8–10} nanotubes can be efficiently produced via a substitution reaction involving carbon nanotubes as templates.^{11,12} Carbon nanotubes and activated carbon have high specific surface areas where the reactant gases (such as boron oxide and nitrogen) can reach. Based on such similarities, we here suggest and successfully demonstrate that the substitution-reaction is suitable for efficiently synthesizing activated BN using activated carbon as a template.

The activated carbon used in this study was obtained commercially from Calgon. The substitution reaction was performed in a horizontal, high-temperature furnace. B₂O₃ powder (Alfa ≥ 99.99%) was placed in an open graphite crucible and then covered with activated carbon. The crucible was held in a flowing nitrogen atmosphere at 1580 °C for 45 min. After the reaction, the B_xC_yN_z intermediate product was collected from the bed of porous carbon.

To determine appropriate experimental parameters for further processing of the intermediate product, we investigated the effect of an oxidizing environment on the pure starting activated carbon and on the B_xC_yN_z intermediate product. Figures 1a and 1b respectively show thermogravimetric analysis (TGA 7, Perkin-Elmer) results for the activated carbon and the B_xC_yN_z intermediate product. The behaviors of the activated carbon and the B_xC_yN_z intermediate product are similar to those of the carbon nanotubes and B_xC_yN_z nanotubes, respectively.¹² These results suggest that the B_xC_yN_z intermediate product is most effectively depleted of carbon between 500 °C and 700 °C.

Thus, our B_xC_yN_z intermediate product was generally further processed by heating in air at 600 °C for 30 min to

* Corresponding author. E-mail: azettl@socrates.berkeley.edu.

[†] Department of Physics, University of California, Berkeley.

[‡] Lawrence Berkeley National Laboratory.

[§] Department of Chemistry, University of California, Berkeley.

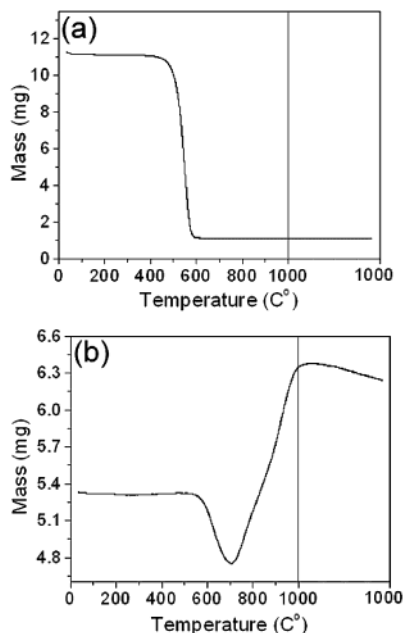


Figure 1. The TGA is heated from room temperature to 1000 °C in an 80% N₂/20% O₂ (by volume) atmosphere at a rate of 3 °C/min and then held at 1000 °C for 2 h. (a) Plot of the mass of activated carbon versus temperature and reaction time. The mass of the activated carbon starts to decrease at about 500 °C, drops to about 9% of its original value between 450 °C and 580 °C, then remains constant up to 1000 °C. The final remaining material consists of impurities. (b) Plot of the mass of B_xC_yN_z intermediate product versus temperature and reaction time. The mass of the B_xC_yN_z intermediate product decreases between 550 °C and 700 °C. In this temperature region, the sample mass decreases by about 12%. Above 700 °C, the mass begins to increase and stabilizes after the sample is held at 1000 °C for short time.

remove any possible remaining carbon and/or convert any synthesized B_xC_yN_z to pure BN.¹² The final resulting samples and starting materials were characterized by conventional scanning electron microscopy (SEM) and high-resolution transmission electron microscopy (HRTEM) using a Philips CM200 FEG equipped with a parallel electron energy-loss spectroscopy detector (EELS, Gatan PEELS 678). The surfaces of the materials were investigated by nitrogen porosimetry (Quantachrome Autosorb-1 series). Surface area measurements were obtained by means of the Brunauer–Emmet–Teller (BET) method.¹³ The pore size distributions were analyzed by the Barrett–Joyner–Halenda (BJH) method.¹⁴

Figure 2 shows SEM images of the starting material and BN product. Figures 2a,b show results for the activated carbon starting material for two different magnifications, while Figures 2c,d show corresponding results for the BN material. At the ~1–10 μm size scale, the carbon-based and BN-based materials have very similar morphologies.

Figure 3 shows HRTEM images, again for the starting material and product. Figures 3a–c show results for activated carbon at successively higher magnification, while Figures 3d–f show corresponding results for the product BN material. At the 80 and 20 nm size scales, the BN-based product is strikingly similar in morphology to the activated

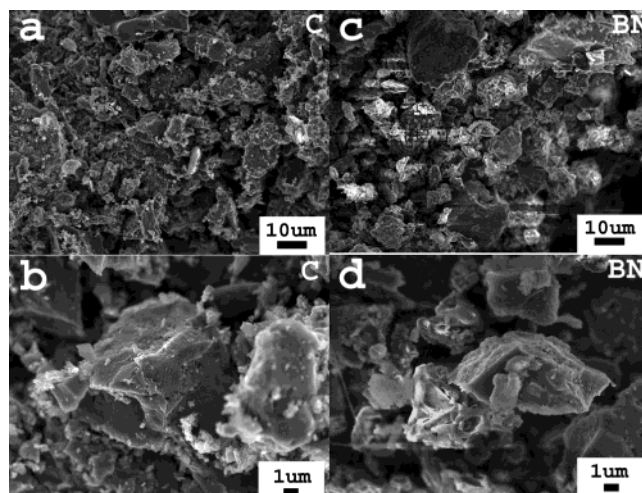


Figure 2. SEM images of starting activated carbon (a, b) and product activated BN (c, d). The overall morphologies of the starting material and product are similar.

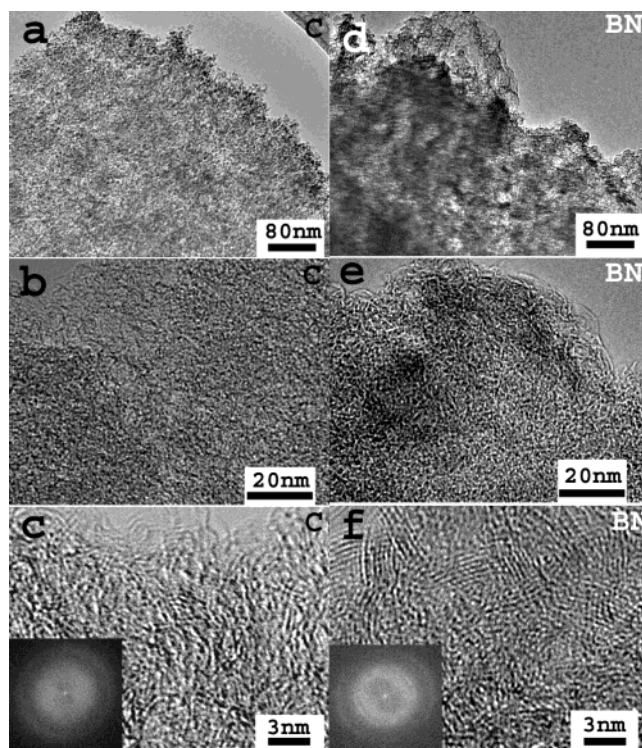


Figure 3. TEM images of starting activated carbon (a–c) and product activated BN (d–f). The insets in (c) and (f) show FFT diffraction patterns of the corresponding high-resolution images.

carbon template. The matrix of both samples consists of a uniform, isotropic microtexture.

Subtle differences between the carbon starting material and the BN-based product are revealed at high magnification, as seen in comparing Figures 3c and 3f. Here the BN-based material shows slightly more “graphitization”, i.e., the degree of activation for the BN system appears less than that of the activated carbon template. Figure 3c shows the pores of activated carbon to be mostly slit-shaped spaces between twisted aromatic sheets.¹ Figure 3c also shows that there are small amounts of graphitic ribbons. A fast Fourier transform (FFT) of the image in Figure 3c is shown as an inset, which

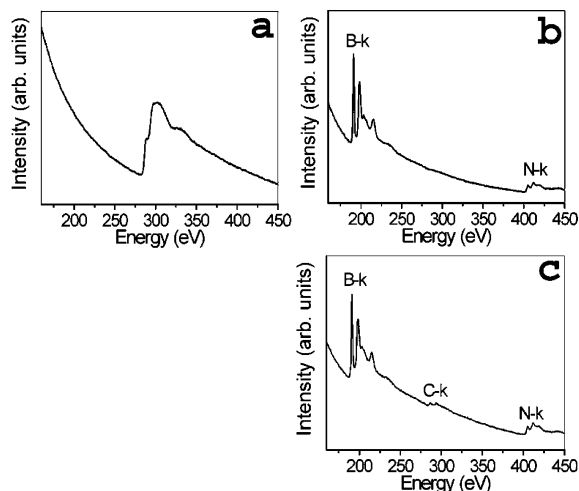


Figure 4. EELS core electron K-shell spectra for (a) the starting activated carbon, and (b, c) the BN-based product. The spectrum in (b) indicated BN in a 1:1 ratio, while (c) indicates $B_xC_yN_z$ with $x/z = 1$ and $y/(x + z) = 0.25$ ratios.

reveals broad fuzzy rings corresponding to the largely amorphous structure of the activated carbon. The corresponding HRTEM image of Figure 3f shows that the BN-based product has more and larger crystalline structure ribbons than the starting activated carbon. The inset of Figure 3f shows the FFT of the associated image. This again shows evidence for fuzzy rings corresponding to significant amorphous structures of the activated BN product, although angular structure in the FFT indicates that the amorphization is not as complete as for activated carbon. XRD measurements were performed which support the conclusion that the BN product has more crystalline structure than the starting activated carbon.

EELS spectra were recorded during HRTEM characterization to confirm the stoichiometry of starting materials and products. Spectra were obtained using a probe beam with a diameter of 5–10 nm. A typical EELS spectrum for the activated carbon starting material is shown in Figure 4a; it reveals the expected distinct C–*k* edge at 284 eV. A typical EELS spectrum for the product, shown in Figure 4b, indicates two distinct absorption features, one starting at 188 eV and the other at 401 eV, corresponding respectively to the known B–*k* and N–*k* edges. The experimental error of about 10% is due mainly to background subtraction when the EELS spectra are analyzed. The extracted atomic B/N ratio is close to 1. Hence most of the porous structures of the products are pure BN. On the other hand, a minority of EELS spectra taken from some product areas indicate the presence of B, N, and C (Figure 4c). This suggests that there exists some porous $B_xC_yN_z$ in the sample. The $y/x + z$ atomic ratio is found to be smaller than 0.25, while the B/N atomic ratio is usually close to 1, implying the carbon content averaged over the whole final product is quite low. No pure carbon area has been detected in the product materials.

The pore structures of the starting activated carbon and the porous BN have been examined via nitrogen absorption experiments to determine the BET surface area, total pore volume, and the average pore. The results are presented in

Table 1. N_2 Porosimetry Data for Porous BN and Starting Porous Carbon

sample	BET surface area (m^2g^{-1})	total pore volume (cm^3g^{-1})	average pore radius (\AA)
porous C	779.0	0.5465	14.03
porous BN	167.8	0.2699	32.16

Table 1. The surface area of the activated BN is $168 m^2/g$, exceeding by at least a factor of 3 that reported for porous BN, whose specific surface area is $50 m^2/g$, produced by the borane-based molecular precursor method.⁶ Total pore volume and average pore radius for the activated BN differ from corresponding parameters for activated carbon by about a factor of 2.

The following chemical reaction is proposed for the conversion of porous pure BN through complete substitution of C atoms by B and N atoms:



Similar to the carbon nanotubes, the spacing among the porous structures of activated carbon is large enough for the passage of N_2 and boron oxide vapor, so the above chemical reactions apply to the entire sample volume. BN nanotubes made by the substitution reaction using carbon nanotubes as templates have a much higher crystalline structure than that of starting carbon nanotubes. Similarly, the activated BN assumes the starting porous carbon structure, but has a higher crystalline structure and has more crystalline structure ribbons. During the high-temperature reaction, some pore structures might be collapsed to some degree. In the activated BN product, there are some crystalline structure BN sheets; these are also found in the product of BN nanotubes made by the conversion of carbon nanotubes. The above factors help explain the differences between surface areas, average pore radius, and total pore volume of the starting material and product.

The Pauling electronegativities of boron and nitrogen in hexagonal BN are 2.0 and 3.0, respectively. The Pauling electronegativity of carbon in graphite is 2.5. Therefore, the (de-)hydriding properties of BN are expected to be different from graphite due to the dissimilar local electronic structure.¹⁵ Recent experiments have indicated that nanostructured hexagonal BN and BN nanotubes have favorable hydrogen storage properties.^{15,16} It is anticipated that the activated BN reported here is also a good candidate for hydrogen storage and also for other porous materials applications.

In summary, the substitution reaction route has been demonstrated as an efficient synthesis route to synthesize activated BN and $B_xC_yN_z$. This simple and easily scalable substitution reaction method could, in principle, produce BN and $B_xC_yN_z$ in any quantity.

Acknowledgment. This research was supported in part by the Office of Energy Research, Office of Basic Energy Science, Division of Materials Sciences, U.S. Department

of Energy (contract DE-AC03-76SF00098) administered through the sp² and Interfacing Nanostructures Initiatives.

References

- (1) Joo, S. H.; Choi, S. J.; Oh, L.; Kwak, J.; Liu, Z.; Terasaki, O.; Ryoo, R. *Nature* **2001**, *412*, 169.
- (2) Bansal, R. C.; Donnet, J.; Stoeckli, F. *Active Carbons*; Marcel Dekker Inc.: New York and Basel, 1988.
- (3) Pouch, J. J.; Alterovitz, S. A. *Synthesis and properties of boron nitride*; Aedermannsdorf: Switzerland: Materials Science forum 1990; vol. 54, 55.
- (4) Narula C. K.; Schaeffer R.; Paine R. T. *J. Am. Chem. Soc.* **1987**, *109*, 5556.
- (5) Borovinskaya, I. P.; Bunin, V. A.; Merzhanov, A. G. *Mendeleev Commun.* **1997**, *2*, 47.
- (6) Perdigon-Melon, J. A.; Auroux, A.; Cornu, D.; Miele, P.; Toury, B.; Bonnetot, B. *J. Org. Chem.* **2002**, *657*, 98.
- (7) Chopra, N. G.; Luyken, R. J.; Cherrey, K.; Crespi, V. H.; Cohen, M. L.; Louie, S. G.; Zettl, A. *Science* **1995**, *269*, 966.
- (8) Han, W. Q.; Bando, Y.; Kurashima, K.; Sato, T. *Jpn. J. Appl. Phys.* **1999**, *38*, L755.
- (9) Golberg, D.; Bando, Y.; Han, W. Q.; Kurashima, K.; Sato, T. *Chem. Phys. Lett.* **1999**, *308*, 337.
- (10) Han, W. Q.; Cumings, J.; Hunag, X.; Bradley, K.; Zettl, A. *Chem. Phys. Lett.* **2001**, *346*, 368.
- (11) Han, W. Q.; Bando, Y.; Kurashima, K.; Sato, T. *Appl. Phys. Lett.* **1998**, *73*, 3085.
- (12) Han, W. Q.; Mickelson, W.; Cumings, J.; Zettl, A. *Appl. Phys. Lett.* **2002**, *81*, 1110.
- (13) Brunauer, S.; Emmett, P. H.; Teller, E. *J. Am. Chem. Soc.* **1938**, *60*, 309.
- (14) Barret, E. P.; Joyner, L. G.; Halenda, P. P. *J. Am. Chem. Soc.* **1951**, *73*, 373.
- (15) Wang, P.; Orimo, S.; Matsushima, T.; Fujii, H. *Appl. Phys. Lett.* **2002**, *80*, 318.
- (16) Han, R.; Bando, Y.; Zhu, H.; Sato, T.; Xu, C.; Wu, D. *J. Am. Chem. Soc.* **2002**, *124*, 7672.

NL034843A